First principles calculations for modern ceramic science and engineering

2008 J. Phys.: Condens. Matter 20 064215

(http://iopscience.iop.org/0953-8984/20/6/064215)

IOP PUBLISHING JOURNAL OF PHYSICS: CONDENSED MATTER

J. Phys.: Condens. Matter **20** (2008) 064215 (6pp) doi:10.1088/0953-8984/20/6/064215

First principles calculations for modern ceramic science and engineering

Isao Tanaka and Fumiyasu Oba

Department of Materials Science and Engineering, Kyoto University, Yoshida, Sakyo, Kyoto 606-8501, Japan

Received 5 September 2007, in final form 21 October 2007
Published 24 January 2008
Online at stacks.iop.org/JPhysCM/20/064215

Abstract

The free energy of compounds can be theoretically obtained as a function of temperature, pressure and chemical potentials by a combination of a first principles method including phonon calculations and statistical approaches using cluster expansion and Monte Carlo simulations. The information is quite useful in ceramic science and engineering since experimental data are not abundantly available. As an example of phonon calculations, results for graphite in comparison to diamond are presented. The free energy difference among polymorphs of Ga_2O_3 is shown as a function of temperature as well. Theoretical calculations of x-ray absorption near edge structures (XANES) and electron energy loss near edge structures (ELNES) are also demonstrated. Proper inclusion of the core–hole effect is mandatory in the calculation. For 3d transition element $L_{2,3}$ XANES/ELNES, a configuration interaction approach to take account of the correlation among the core–hole and the excited electron satisfactorily reproduces experimental spectra. As an example, results for Mn-doped ZnO are shown.

(Some figures in this article are in colour only in the electronic version)

1. Introduction

Ceramic materials are widely used in modern technology. They are used for energy conversion devices such as fuel cells and lithium batteries, photoemission devices for information technology, catalysts for environmental issues, structural components and semiconductors to mention a few examples. Compared to metallic alloys forming simple close-packed structures, ceramic crystals often exhibit more complicated open structures having multiple atomic sites with different local environments. They are therefore more difficult to examine by theoretical methods. Moreover, less experimental information is available for ceramic crystals as compared to the common metals. In the present authors' group, efforts to combine experimental works and first principles calculations have been made in order to reveal fundamental structure–property relationships in ceramic materials. Some our recent works are surveyed in this paper.

2. Stability and structures of complex crystals

Modern materials science is described with statistical thermodynamics. The free energy of compounds and its temperature/pressure dependence is indispensable information. One can predict the ultimate products of reactions on the basis of free energy. Using first principles calculations, however, internal energy at zero temperature was the only quantity that could be routinely computed until recently. First principles theorists have often been overly criticized that the zero temperature quantities are not compatible with materials science issues.

A number of phenomena contribute to the temperature dependence of the free energy in general. The common term in all crystals is the contribution of lattice vibration. Quasi-harmonic approximation is often used to take account of it, including thermal expansion effects. Once the phonon density of states (DOS) $g(\nu)$ is known, the vibrational contribution to the free energy is obtained as

$$F_{\mathrm{vib}} = 3nk_{\mathrm{B}}T \int_0^\infty \mathrm{d}\nu\, g(\nu) \ln[2\sinh(h\nu/2k_{\mathrm{B}}T)], \quad (1)$$

where n is the number of atoms in the periodic unit. The heat capacity at constant volume C_V is given by integrating the product of $g(\nu)$ and the weighting factor $W(h\nu/k_{\mathrm{B}}T) = (h\nu/k_{\mathrm{B}}T)^2 \exp(h\nu/k_{\mathrm{B}}T)/(\exp(h\nu/k_{\mathrm{B}}T) - 1)^2$ as

$$C_V = 3nk_{\mathrm{B}} \int_0^\infty \mathrm{d}\nu\, g(\nu) W(h\nu/k_{\mathrm{B}}T). \quad (2)$$

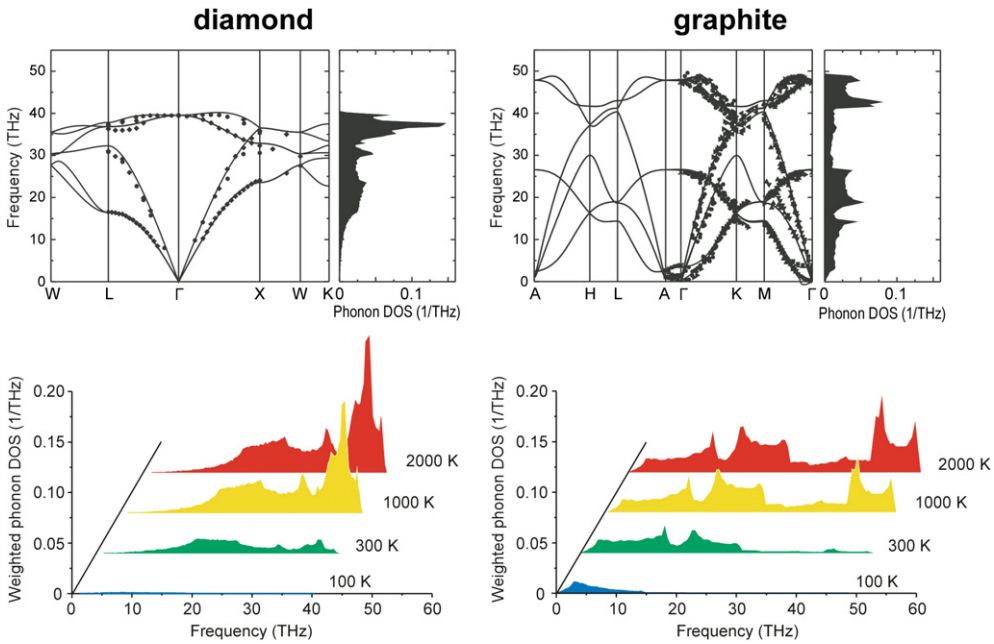

Figure 1. Upper: phonon dispersion relations and phonon density of states (DOS) of diamond and graphite. Solid curves show the calculated dispersions. Experimental values from different data sources are denoted by different symbols [8–16]. Lower: weighted phonon DOS at several temperatures.

Figure 1 (upper) shows theoretical phonon dispersion relation and $g(\nu)$ for diamond and graphite [1] obtained using the frozen-phonon method combined with first principles calculations within the local density approximation (LDA) [2, 3], which were performed using the projector augmented wave (PAW) method [4] as implemented in the VASP code [5–7]. Agreement of the calculated phonon frequencies with the experiments is quite satisfactory. The temperature variation of the integrand in the formula for the heat capacity, $g(\nu)W(h\nu/k_{\mathrm{B}}T)$, is shown in figure 1 (lower). The weighting factor $W(h\nu/k_{\mathrm{B}}T)$ represents what proportion of the vibrational states can be excited and contribute to the lattice heat capacity. At 100 K, for instance, $W(h\nu/k_{\mathrm{B}}T)$ is less than 1% in the frequency region above 20 THz. Only low frequency states contribute to the heat capacity at low temperatures. Since graphite has much more vibrational states in the low frequency region than diamond does, graphite exhibits a larger heat capacity than diamond at low temperatures. At an elevated temperature of 1000 K, on the other hand, almost all vibrational states in the whole frequency range are excited in both crystals.

Ceramic crystals often show a number of polymorphs. Not only the intrinsic properties of crystals as exemplified by heat capacity, but also extrinsic properties such as behavior of dopants are sometimes markedly dependent on the crystal structure. Information about structure–property relationships among polymorphs is therefore of great interest for ceramic science. The energetical hierarchy of polymorphs can be discussed with the free energy. However, experimental data for the free energy difference among polymorphs are rarely available.

We have obtained theoretical free energy differences among polymorphs in selected ceramic materials such as ZrO_2 [17], Ga_2O_3 [18] and Si_3N_4 [19]. Pressure-induced rhombohedral to cubic phase transformation of perovskite oxides was systematically investigated in [20]. Among Ga_2O_3 polymorphs, the monoclinic β-phase is known to form under ordinary conditions. Depending on synthesis conditions, four other phases with different structures have been reported, namely α, γ, δ and ε phases. However, their energetical hierarchy was not reported. The structure of the ε-phase was not known, either. In [18] we determined the crystal structure of ε-Ga_2O_3 using the PAW method with the generalized gradient approximation (GGA) [21]. The space group of $Pna2_1$ (no. 33, orthorhombic) was adopted, which is the same as that of κ-Al_2O_3 and ε-Fe_2O_3. Then the energetical hierarchy of polymorphs was discussed through total energy and frozen phonon calculations.

Figure 2 shows the theoretical free energy of four Ga_2O_3 phases relative to the β-phase as a function of temperature [18]. The γ-phase has a defective spinel structure in which the positions of vacant sites are not clearly known. The result of the γ-phase is shown only at zero temperature, which corresponds to the configuration showing the lowest energy among the 14 vacant-site arrangements within 40-atom supercells. The free energies are $\beta < \varepsilon < \alpha < \delta < \gamma$ at low temperatures. With the increase of temperature, the difference in free energy between the β-phase and the ε-phase becomes smaller, and disappears at around 1600 K.

The second important contribution to the free energy comes from the configurational entropy, which is determined by the number of configurations in which atoms and defects are arranged on given lattice sites. The configurational entropy has been computed analytically by adopting some geometric models. The cluster variation method [22] is a typical example. We have constructed a pseudo-binary

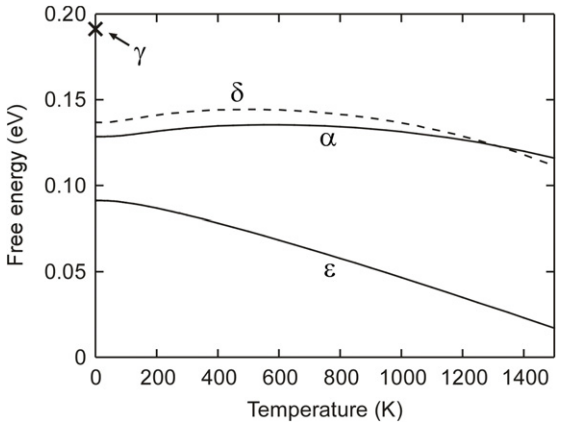

Figure 2. Temperature dependence of Helmholtz free energy per formula unit for α-, γ- δ- and ε-Ga_2O_3 with respect to β-Ga_2O_3.

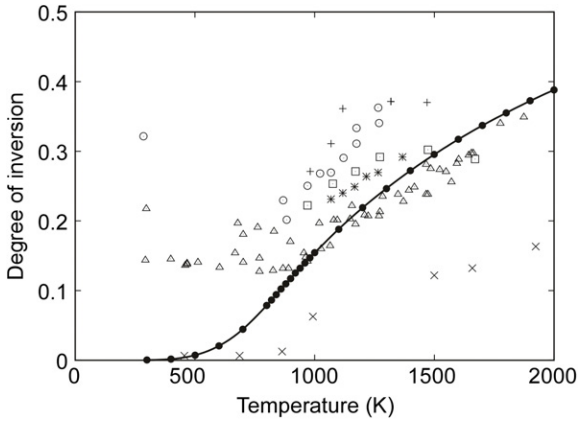

Figure 3. Calculated temperature dependence of the degree of inversion x in $(Mg_{1-x}Al_x)[Mg_xAl_{2-x}]O_4$ (solid curve and closed circles) compared with experimental values (other symbols) [26–31].

phase diagram for MgO–ZnO using a combination of the cluster expansion and cluster variation method, and first principles calculations [23]. Vibrational free energy obtained by frozen-phonon calculations was included. The temperature and pressure dependence of the solid solubility of two oxides was predicted. For more complicated structures, the cluster variation approach is typically not suitable. Instead of that, Monte Carlo simulations can be used to take account of the configuration contribution numerically. Using a combination of first principles calculations, a cluster expansion and canonical Monte Carlo simulations, we have systematically investigated the temperature dependence of cationic disorder in AB_2O_4 spinel, where A and B are divalent and trivalent cations, respectively [24, 25]. Figure 3 shows the temperature dependence of the degree of inversion x in $(Mg_{1-x}Al_x)[Mg_xAl_{2-x}]O_4$ along with experimental data obtained by neutron diffraction, x-ray diffraction and NMR [24, 26–31]. Although the experimental data are widely scattered, the theoretical curve fell on them. By the theoretical calculations, $MgAl_2O_4$ is confirmed to be normal spinel ($x = 0$) at zero temperature. The predicted order–disorder transition temperature of $MgAl_2O_4$ is 860 K, which well agrees with the experimental one ranging from 870 to 950 K [31–33]. A similar combined method of first principles calculations and cluster expansion was recently applied to elucidate the structures and stabilities of a series of non-stoichiometric SnO_{2-x} compounds, which are as yet unknown experimentally [34].

3. XANES and ELNES for ceramic science

Both XANES (x-ray absorption near edge structures) and ELNES (electron energy loss near edge structures) are important tools in ceramic science and engineering offering information on the local environment of selected elements not only in crystals but also in amorphous materials. Recent technological progress enables measurements of XANES for ppm-level dopants using modern synchrotron facilities [35]. Combined with transmission electron microscopy, ELNES can be used to analyze the local structures with sub-nanometer spatial resolution [36].

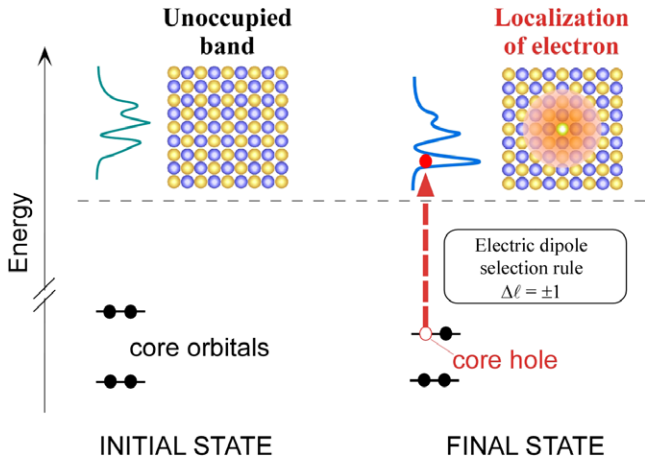

Figure 4. Schematic illustration of the electronic transition relevant to XANES/ELNES.

Figure 4 schematically illustrates the origin of XANES/ELNES. Basically it corresponds to the electronic transition from a core state to unoccupied states. Because of the presence of the core–hole, the electronic structure at the final state of the transition is different from that of the initial state or the ground state before the transition. Generally speaking, the wavefunction is localized at the core–holed atom. As a result, XANES often shows a sharp peak near the absorption edge which is not present in the DOS at the ground state. Proper inclusion of the core–hole effect is necessary for the reproduction of XANES using first principles calculations.

The photo-absorption coefficient, μ, or photo-absorption cross section (PACS) can be generally described by Fermi's 'golden rule' as

$$\mu \propto \sum_{\mathrm{f}} |\langle \psi_{\mathrm{f}} | \exp(\mathrm{i}\mathbf{k}\cdot\mathbf{r})\cdot\mathbf{e}\cdot\mathbf{P}|\psi_{\mathrm{i}}\rangle|^2 \delta(\hbar\omega - E_{\mathrm{f}} + E_{\mathrm{i}}), \quad (3)$$

where ψ_{f} and ψ_{i} are many-electron wavefunctions at the final and initial states, respectively. E_{f} and E_{i} are the total energies of the corresponding states. $\hbar\omega$, $\mathbf{k}$, and $\mathbf{e}$ are the

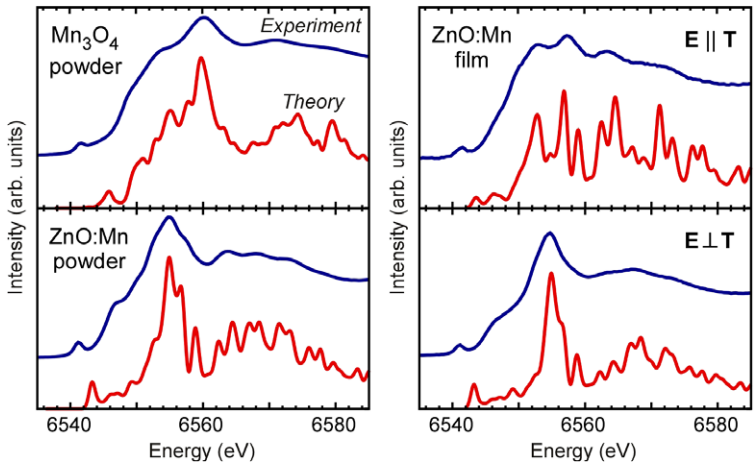

Figure 5. Experimental and theoretical Mn K-edge XANES for ZnO:Mn and Mn_3O_4.

energy, wavevector and the unit vector for the polarization direction of the x-ray. **P** is the sum of the linear momentum operators of electrons. Regarding XANES, the equation can be approximated using the one-electron wavefunctions of the core state, ϕ_i, and the excited electron, ϕ_f, as

$$\mu \propto \sum_f (|\langle\phi_f|\mathbf{e}\cdot\mathbf{r}|\phi_i\rangle|^2 + \tfrac{1}{4}|\langle\phi_f|(\mathbf{e}\cdot\mathbf{r})(\mathbf{k}\cdot\mathbf{r})|\phi_i\rangle|^2) \times \delta(\hbar\omega - E_f + E_i), \quad (4)$$

where **r** is the position of the excited electron. However, one should pay great attention to include the core–hole effects. The electronic relaxation associated with the presence of the core–hole at the final state and additional correlation between the core–hole and the excited electron need to be accounted for if one wants to reproduce the experimental spectra using equation (4).

The first term in the parenthesis of equation (4) is usually dominant for XANES because $\mathbf{k}\cdot\mathbf{r} \ll 1$. This term corresponds to the electric dipole transition. The second term that shows an electric quadrupole transition is almost negligible in most cases. Under the dipole approximation, the equation (4) can be further simplified to be

$$\mu \propto \sum_f |\langle\phi_f|\mathbf{e}\cdot\mathbf{r}|\phi_i\rangle|^2\delta(\hbar\omega - E_f + E_i). \quad (5)$$

The intensity of ELNES within the dipole approximation can be described by

$$I \propto \sum_f |\langle\phi_f|\mathbf{q}\cdot\mathbf{r}|\phi_i\rangle|^2\delta(\hbar\omega - E_f + E_i), \quad (6)$$

where **q** is the scattering vector or momentum transfer of the incident electron, and is assumed to be small. $\hbar\omega$ is the electron energy loss in this case. As can be understood by the analogy of equations (5) and (6), the scattering vector **q** for ELNES plays the same role as the polarization vector **e** in XANES. Two spectra are comparable and the computational procedure to obtain theoretical spectra is therefore identical.

First principles methods to reproduce and interpret the spectra have been established recently. When a core–hole is adequately taken into account, most of the K-edge spectra can be well reproduced using a modern band-structure method within the one-electron approximation [37, 38]. On the other hand, many-electron calculations are mandatory to reproduce $L_{2,3}$-edge spectra of 3d transition-metal elements because of strong correlations among 3d electrons and a 2p hole. We have developed a configuration interaction (CI) approach using model clusters to obtain theoretical $L_{2,3}$-edge spectra in a first principles manner [39–41]. This was successful in reproducing experimental XANES/ELNES systematically.

Diluted magnetic semiconductors (DMS) have been extensively studied for over a decade. Recently DMS showing room temperature ferromagnetism were reported for several systems including ZnO:Mn [42] and GaN:Mn [43]. However, the mechanism of ferromagnetism is still controversial, which can be mainly ascribed to the lack of detailed information on the atomic scale environment of Mn dopants. In our group, the ZnO:Mn system has been studied by means of Mn-K and Mn-$L_{2,3}$ XANES in conjunction with first principles calculations [44–46]. Polycrystalline powder (0.01–20 at.% Mn) and pulsed-laser deposited films (5 at.% Mn) on the sapphire (0001) plane have been examined. By x-ray diffraction, Mn was found to dissolve into ZnO up to 5 at.% in the polycrystal samples. The presence of Mn_3O_4 was apparent only for samples with a higher Mn content. The films exhibit a single crystalline phase with the [0001] direction of the wurtzite crystal oriented parallel to the substrate normal.

Figure 5 shows experimental and theoretical Mn-K XANES for the ZnO:Mn powder and thin film with 5 at.% Mn, together with those for Mn_3O_4 as a reference [44]. The theoretical spectra were obtained with the GGA using full-potential augmented plane wave plus local orbitals (APW + lo) calculations [47]. Neutral supercells of 108 atoms for ZnO:Mn and 112 atoms for Mn_3O_4, with and without core–holes, were used in the calculation. The former corresponds to the formal charge of Mn being +2. Spin polarization was taken into account. Absolute transition energies of all theoretical spectra are shifted by −20 eV (−0.3%). The theoretical spectra are in good agreement with the experimental spectra, including the orientation dependence for the thin film, i.e. the electric field **E** parallel or perpendicular to the film/substrate

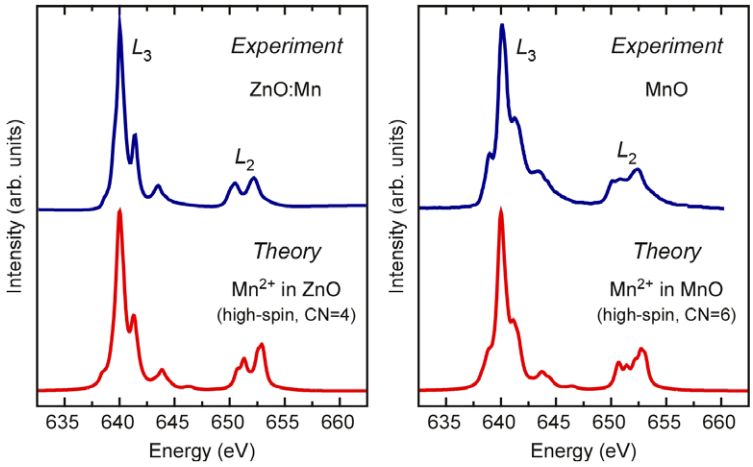

Figure 6. Experimental and theoretical Mn $L_{2,3}$-edge XANES for ZnO:Mn and MnO. The experimental spectrum for MnO is taken from [48]. CN denotes the coordination number of Mn.

normal **T**. For the ZnO:Mn powder, it was found that the Mn-*K* XANES does not change in the range of Mn concentration from 0.01 to 5 at.%. Absence of Mn_3O_4 components is evident for both ZnO:Mn powder and thin film, which confirms the x-ray diffraction results. From the Mn-*K* XANES analysis, we can conclude that Mn^{2+} is substitutionally present in ZnO up to 5 at.% Mn without significant clustering or ordering.

Figure 6 shows experimental Mn-$L_{2,3}$ XANES for ZnO:Mn and MnO with theoretical spectra obtained using CI calculations [45, 46]. $[MnO_4]^{6-}$ and $[MnO_6]^{10-}$ model clusters, embedded in an array of ± 2 point charges located at the atomic positions of the ZnO and MnO crystals, respectively, were employed. Many-electron wavefunctions were expressed as a linear combination of Slater determinants composed of Mn-2p, Mn-3d and O-2p based relativistic molecular orbitals. The agreement between experimental and theoretical spectra is very satisfactory for both ZnO:Mn and MnO. The presence of satellite peaks in L_3 at both lower and higher energy sides is well reproduced. This supports the conclusion obtained from the Mn-*K* XANES analysis for ZnO:Mn, i.e. the substitution of Mn^{2+} for Zn. The same method has been applied to analyze Mn-$L_{2,3}$ XANES for GaN:Mn [46, 49] and Ga_2O_3:Mn [50] to reveal the valence and spin state of Mn dopants.

4. Conclusions

Statistical thermodynamics is the common language in materials science and engineering. Recent progress with first principles calculations has enabled quantitative evaluation of the free energy of a system at given temperature, pressure and chemical potentials with reliable precision. Phonon calculations and the cluster expansion approach are demonstrated as emerging tools to take account of the temperature dependence of the free energy from first principles. XANES/ELNES play very important roles in modern materials characterization. Taking account of the correlation among the core–hole and the excited electron, one can reproduce the spectra satisfactorily. Examples of such calculations are given for the ZnO:Mn system at both Mn-*K* and Mn-$L_{2,3}$ edges. From the viewpoints of ceramic science and engineering, the first principles method is now no longer a piece of magic exclusively dreamt up by theorists but is an essential tool for the research and development of advanced materials.

Acknowledgments

This work was supported by three programs from the Ministry of Education, Culture, Sports, Science and Technology of Japan. They are the Grant-in-Aid for Exploratory Research, Scientific Research (A), and Priority Area on ‘Atomic Scale Modification’, no. 474.

References

[1] Tohei T, Kuwabara A, Oba F and Tanaka I 2006 *Phys. Rev.* B **73** 064304
[2] Ceperley D M and Alder B J 1980 *Phys. Rev. Lett.* **45** 566
[3] Perdew J P and Zunger A 1981 *Phys. Rev.* B **23** 5048
[4] Blöchl P E 1994 *Phys. Rev.* B **50** 17953
[5] Kresse G and Hafner J 1993 *Phys. Rev.* B **48** 13115
[6] Kresse G and Furthmüller J 1996 *Phys. Rev.* B **54** 11169
[7] Kresse G and Joubert J 1999 *Phys. Rev.* B **59** 1758
[8] Warren J L, Yarnell J L, Dolling G and Cowley R A 1967 *Phys. Rev.* **158** 805
[9] Schwoerer-Bohning M, Macrander A T and Arms D O 1998 *Phys. Rev. Lett.* **80** 5572
[10] Maultzsch J, Reich S, Thomsen C, Requardt H and Ordejon P 2004 *Phys. Rev. Lett.* **92** 075501
[11] Wilkes J L, Palmer R E and Willis R F 1987 *J. Electron Spectrosc. Relat. Phenom.* **44** 355
[12] Siebentritt S, Pues R, Rieder K H and Shikin A M 1997 *Phys. Rev.* B **55** 7927
[13] Nicklow R, Wakabayashi N and Smith H G 1972 *Phys. Rev.* B **5** 4951
[14] Oshima C, Aizawa T, Souda R and Ishizawa Y 1988 *Solid State Commun.* **65** 1601
[15] Yanagisawa H, Tanaka T, Ishida Y, Matsue M, Rokuta E, Otani S and Oshima C 2005 *Surf. Interface Anal.* **37** 133
[16] Al-Jishi R and Dresselhaus G 1982 *Phys. Rev.* B **26** 4514

[17] Kuwabara A, Tohei T, Yamamoto T and Tanaka I 2005 *Phys. Rev.* B **71** 064301
[18] Yoshioka S, Hayashi H, Kuwabara A, Oba F, Matsunaga K and Tanaka I 2007 *J. Phys.: Condens. Matter* **19** 346211
[19] Kuwabara A and Tanaka I 2005 unpublished
[20] Tohei T, Kuwabara A, Yamamoto T, Oba F and Tanaka I 2005 *Phys. Rev. Lett.* **94** 035502
[21] Perdew J P, Burke K and Ernzerhof M 1996 *Phys. Rev. Lett.* **77** 3865
[22] Kikuchi R 1951 *Phys. Rev.* **81** 988
[23] Seko A, Oba F, Kuwabara A and Tanaka I 2005 *Phys. Rev.* B **72** 024107
[24] Seko A, Yuge K, Oba F, Kuwabara A, Tanaka I and Yamamoto T 2006 *Phys. Rev.* B **73** 094116
[25] Seko A, Yuge K, Oba F, Kuwabara A and Tanaka I 2006 *Phys. Rev.* B **73** 184117
[26] Peterson R C, Lager G A and Hitterman R L 1991 *Am. Mineral.* **76** 1455
[27] Redfern S A T, Harrison R J, O'Neill H S C and Wood D R R 1999 *Am. Mineral.* **84** 299
[28] Andreozzi G B, Princivalle F, Skogby H and Giusta A D 2000 *Am. Mineral.* **85** 1164
[29] Wood B J, Kirkpatrick R J and Montez B 1986 *Am. Mineral.* **71** 999
[30] Millard R L, Peterson R C and Hunter B K 1992 *Am. Mineral.* **77** 44
[31] Yamanaka T and Takeuchi Y 1983 *Kristallografiya* **165** 65
[32] Weeks R A and Sonder E 1979 *J. Am. Chem. Soc.* **82** 92
[33] Suzuki I and Kumazawa M 1980 *Phys. Chem. Minerals* **5** 279
[34] Seko A, Togo A, Oba F and Tanaka I 2007 submitted
[35] Tanaka I *et al* 2003 *Nat. Mater.* **2** 541
[36] Batson P E 1993 *Nature* **366** 727
[37] Tanaka I, Mizoguchi T and Yamamoto T 2005 *J. Am. Ceram. Soc.* **88** 2013
[38] Mizoguchi T, Tanaka I, Yoshioka S, Kunisu M, Yamamoto T and Ching W Y 2004 *Phys. Rev.* B **70** 045103
[39] Ogasawara K, Iwata T, Koyama Y, Ishii T, Tanaka I and Adachi H 2001 *Phys. Rev.* B **64** 115413
[40] Ikeno H, Tanaka I, Koyama Y, Mizoguchi T and Ogasawara K 2005 *Phys. Rev.* B **72** 075123
[41] Ikeno H, Mizoguchi T, Koyama Y, Kumagai Y and Tanaka I 2006 *Ultramicroscopy* **106** 970
[42] Sharma P, Gupta A, Rao K V, Owens F J, Sharma R, Ahuja R, Osorio Guillen J M, Johansson B and Gehring G A 2003 *Nat. Mater.* **2** 673
[43] Sonoda S, Shimizu S, Sasaki T, Yamamoto Y and Hori H 2002 *J. Cryst. Growth* **237–239** 1358
[44] Kunisu M, Oba F, Ikeno H, Tanaka I and Yamamoto T 2005 *Appl. Phys. Lett.* **86** 121902
[45] Ikeno H, Oba F, Kunisu M, Tanaka I and Yamamoto T 2005 unpublished
[46] Sonoda S *et al* 2006 *J. Phys.: Condens. Matter* **18** 4615
[47] Blaha P, Schwarz K, Madsen G, Kvasicka D and Luitz J 2001 *WIEN2k, An Augmented Plane Wave + Local Orbital Program for Calculating Crystal Properties* (Techn. Universitat Wien, Austria)
[48] Gilbert B, Frazer B H, Belz A, Conrad P G, Nealson K H, Haskel D, Lang J C, Srajer G and De Stasio G 2003 *J. Phys. Chem.* A **107** 2839
[49] Sonoda S *et al* 2007 *Appl. Phys. Lett.* **90** 012504
[50] Hayashi H, Huang R, Ikeno H, Oba F, Yoshioka S, Tanaka I and Sonoda S 2006 *Appl. Phys. Lett.* **89** 181903